The 4th International Conference on Structural Health Monitoring and Integrity Management

Virtual Time-reversal Tomography for Impact Damage Detection in Self-sensing Piezoelectric Composite Plates

Junzhen Wang[1] and Yanfeng Shen[1, *]

Abstract: Piezoelectric materials have been widely applied in actuation and sensing device for Structural Health Monitoring (SHM). Composite materials are taking a more and more important role in load-bearing components due to their high-strength, low-weight properties in aerospace engineering. By distributing piezoelectric properties throughout the composite structural component, each location of the material can be used as an actuator and a sensor to generate and receive ultrasonic waves. This enables the construction of dense interrogation probe arrays for active and high-resolution structural sensing. This paper presents the virtual time-reversal tomography for impact damage detection in self-sensing piezoelectric composite plates. A systematic numerical investigation of ultrasonic guided-wave dynamics in anisotropic piezoelectric composite plates is first conducted. The guided wave generation mechanism and characteristics are studied using the harmonic analysis of a finite element model simulating the tuning procedure. Subsequently, an impact damage is introduced and modelled as a group of cone shape delaminations and stiffness losses within the laminate layers through the thickness direction, so as to approximate the practical impact damage. 3D transient dynamic coupled-field finite element models are further adopted to simulate the procedure of guided wave generation, propagation, interaction with the impact damage, and reception in a piezoelectric composite laminate. The contact dynamics are considered to capture the possible nonlinear interactions between guided waves and the impact damage, which would induce Contact Acoustic Nonlinearity (CAN) into the guided waves. Furthermore, the wave damage interaction coefficients (WDICs) are adopted to depict the scattering patterns of guided waves, from which the sensitive wave-path directions can be inferred for active sensing array design. Finally, the predictive simulation signals from the 3D finite element models are fed into the virtual time-reversal probabilistic tomography algorithm to locate and image the impact damage zones. This paper finishes with summary, concluding remarks, and suggestions for future work.

Keywords: Piezoelectric composite, guided waves, impact damage, virtual time reversal, structural health monitoring, delamination, smart structures

[1]University of Michigan-Shanghai Jiao Tong University Joint Institute, Shanghai Jiao Tong University, 800 Dongchuan Road, Minhang District, Shanghai, 200240, China.

[*]Corresponding Author: Yanfeng Shen. Email: yanfeng.shen@sjtu.edu.cn.

1. Introduction

Piezoelectric materials have been widely used as actuation and sensing device in Structural Health Monitoring (SHM) and Nondestructive Evaluation (NDE) applications. For example, piezoelectric wafer active sensors (PWAS) can be mounted on the surfaces of host structures for crack detection [Giurgiutiu (2005)]. On the other hand, composite materials are taking a more and more important role in load-bearing structural components due to their attractive properties such as the high strength, high stiffness, and light weight features. Research efforts have been exerted on combining the merits of both materials to establish structural self-awareness. Haghiashtiani et al. [Haghiashtiani (2014)] made polyvinylidene difluoride (PVDF) matrix composite to realize the integrated sensing capability within the host structure. Minakuchi et al. [Minakuchi (2013)] used embedded optical fiber sensors, achieving distributed sensing purposes to detect damage in large-scale composite structures. In the authors' preliminary study, piezoelectric composite materials have been investigated to transmit and receive guided waves; a synthetic time-reversal method was used to achieve damage imaging [Wang and Shen (2018)].

Lamb wave time reversal method has been investigated as a powerful method for baseline-free damage detection. Cai et al. [Cai (2011)] adopted virtual time reversal (VTR)-based imaging method, improving the spatial resolution of Lamb wave detection. Liu et al. [Liu (2015)] proposed a baseline-free delamination inspection technique for composite plates utilizing air-coupled Lamb wave scans and the VTR algorithm. In this paper, the impact damage is introduced as a group of cone shape delaminations and stiffness loss within the layers through the thickness direction. By inducing CAN, the nonlinear interaction between guided waves and the impact damage can be captured. In addition, the WDICs of impact damage are supposed to provide scattering information for active sensing array design. Finally, the baseline-free VTR probabilistic imaging algorithm is used to locate and image the impact damage zones.

2. Dispersion Relations of Guided Waves in Piezoelectric Composites

An in-depth understanding of the guided wave dispersion features may provide guideline information for SHM system design. The dispersion curves of guided waves in an anisotropic piezoelectric composite plate is obtained using finite element modal analysis with Bloch-Floquet boundary condition. Aberg et al. [Aberg and Gudmundson (1997)] proposed the computation of dispersion curves and mode shapes by periodic boundary conditions. Zhu and Fang further demonstrated the use of standard finite element codes to attain the dispersion curves [Zhu and Fang (2014)]. Similarly, the piezoelectric composite can be treated as the assembly of piezoelectric unit cells.

Figure 1 shows the group velocity curves and directivity wave curves in the 2 mm thick $[0/45]_s$ cross-ply piezoelectric composite plate. Figure 1a and Figure 1b present the group velocity curves in 0° and 90° directions. It can be observed that, within relatively low frequency range, only three fundamental wave modes exist, namely fundamental symmetric mode (S0), fundamental shear horizontal mode (SH0), and fundamental antisymmetric mode (A0). The S0 mode is not heavily dispersive and has a

comparatively high propagation speed. The A0 mode, on the other hand, is highly dispersive, but in the 90° direction, the A0 wave speed becomes much low than that in the 0° direction. The SH0 mode is non-dispersive and has the constant group velocity at around 2000 m/s. The directivity of the wave curves (group velocity) at 100 kHz is plotted in Figure 1c. The wave curves represent the spatial wave propagation pattern. It can be observed that S0 has the highest propagation speed forming a circular pattern along all the directions. While the wave speeds of A0 and SH0 mode exhibit elliptical wave fronts, which change with their propagation directions. In 0° direction, the wave speed of A0 is higher than that of SH0, but SH0 mode wave propagates much faster than A0 mode wave in 90° direction.

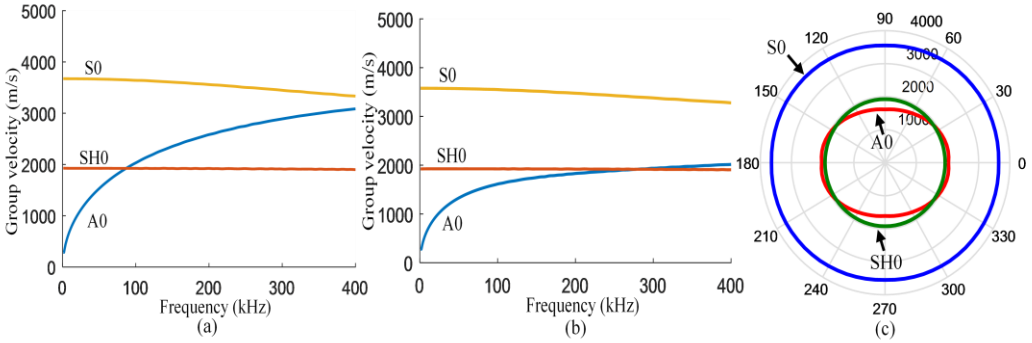

Figure 1: Guided waves in a 2-mm thick $[0/45]_s$ cross-ply piezoelectric composite plate: (a) group velocity curves along 0° direction; (b) group velocity curves along 90° direction; (c) wave curves (group velocity directivity curves) at 100 kHz.

3. Guided Wave Generation and Reception Characteristics

The traditional method to investigate the guided wave generation and reception characteristics is via tuning experiments, where pitch-catch method is adopted to collect signals from transducers. PWAS are amounted on the surfaces of host structures, and excited sweeping a span of frequencies, the amplitudes of multimodal guided waves are recorded. In this study, the FEM has been adopted to obtain the wave generation and reception characteristics in a 2-mm thick $[0/45]_s$ cross-ply piezoelectric composite plate.

The tuning model was constructed to extract the wave amplitude information via harmonic analysis as shown in Figure 2a. Non-reflective boundary (NRB) was implemented on both ends of the plate to eliminate boundary reflections. The green line on the upper surface depicts the excitation and sensing electrodes, which was coupled to apply and receive the excitation and sensing voltage individually. And the bottom green line represents another electrode whose electric potential was set to 0, simulating the grounding condition. In order to ensure an efficient computational accuracy, the frequency extrema at both low and high ends should be treated carefully. The numerical model requires all waves be absorbed efficiently by the NRB, which imposes the demand for the length of NRB region, i.e. the NRB coverage should exceed twice the maximum

wavelength of guided wave mode under consideration. The longest wavelength happens at the low extrema of the frequency range. At 20 kHz, the longest wave length arises from the S0 mode at 200mm. Thus, the NRB region was set to 400 mm. On the other hand, at the high extrema of the frequency range, the shortest wave length comes into play. The accuracy of FEM prediction requires the mesh size should smaller than 1/20th of the shortest wavelength. Up to 400 kHz, the shortest wavelength happens in A0 mode, rendering a value of 4mm. Thus, the element size was set to 0.2 mm. Therefore, the computational accuracy for guided wave generation and reception characteristics between 20 kHz to 400 kHz can be guaranteed.

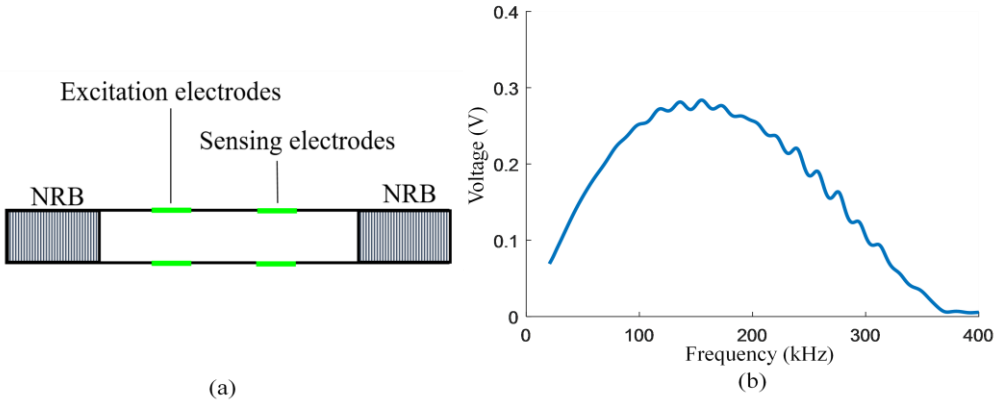

Figure 2: Tuning results: (a) guided wave tuning model; (b) guided wave generation and reception characteristics in a 2-mm thick piezoelectric composite plate.

Figure 2b illustrates the guided wave tuning characteristics in the 2-mm thick $[0/45]_s$ cross-ply piezoelectric composite plate. The voltage from sensing electrodes first rises and then falls down from low frequency to high frequency. It can be observed that the curve is not so smooth but with waviness among certain frequency span, the reason for which is due to the local electro-mechanical resonance between the excitation and sensing electrodes. In addition, it provides the tuning information to select rational excitation frequency for the transient dynamic analysis in the following paragraphs.

4. Impact Damage Model Considering Contact Acoustic Nonlinearity

Impact damage detection is an important issue for the maintenance of aircraft and space structures. The methods used for impact damage detection has been explored for years in within SHM and NDE community. Aymerich et al. [Aymerich and Staszewski (2010)] used nonlinear acoustics to detect impact damage in composite materials. The sideband phenomenon was apparent using a high-frequency interaction between an ultrasonic wave and a low-frequency vibration. Patra et al. [Patra and Banerjee (2017)] proposed using coda wave to detect precursor damage state.

In this study, 3D transient dynamic coupled-field finite element models were constructed to simulate the procedure of guided wave generation, propagation, interaction with the impact damage, and reception in a piezoelectric composite plate. On the other hand,

contact dynamics are considered to capture the possible nonlinear interactions between guided waves and the impact damage, which would induce CAN into the guided waves. It has been reported as a sensitive and powerful approach to detecting delamination and impact damage.

4.1. 3D Model of the Impact Damage

A model of cone shape delaminated layers and stiffness losses within the layers through the thickness direction was constructed, in order to approximate the practical impact damage, which is shown in Figure 3. In the thickness direction, the area of delamination increases, while the apparent material stiffness loss decrease. According to the CT scan image of the impact damage, the delamination and matrix cracks exist in the thickness direction. However, considering the complexity of model, the contact surfaces are only built along the horizontal direction and the vertical matrix crack scatters are modelled via the stiffness loss. SOLID5 coupled field element was deployed to discretize the simulation domain. Extended region of absorbing layers with increasing damping (ALID) was implemented surrounding the plate to eliminate boundary reflections. A 200-Vpp 5-count Hanning window modulated sine tone burst signal centered at 100 kHz was applied on the actuation electrode. To solve the problem accurately and efficiently, the mesh size and time step were optimized. The element size was set 2 mm, which can guarantee enough points to depict up to the second harmonic frequency (200 kHz) wavelength. The time step was set to 0.25 μs, which also satisfies the temporal discretization of the second higher harmonic component. In the thickness direction, the mesh size of 0.5 mm was adopted to depict each layer of composite lamina.

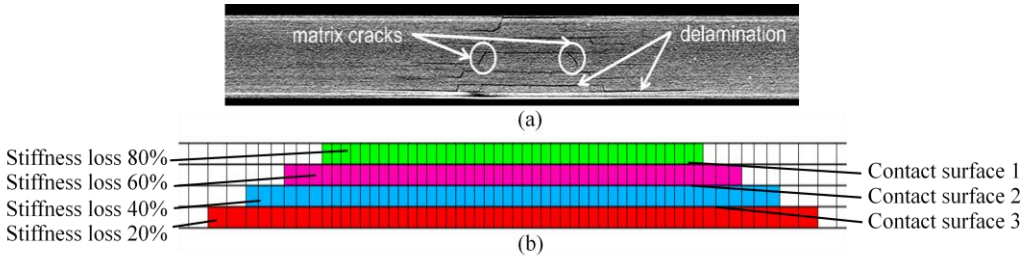

Figure 3: Details of the impact damage model: (a) CT scan image performed by UT Arlington in collaboration with Active Aeroelasticity and Structures Research Laboratory at the University of Michigan; (b) cross-section of 3D impact damage model.

For the contact analysis, the contact pair was established using contact elements (TARGE170 and CONTA174). The thermal-electrical coupling contact was activated. A penalty algorithm was deployed. Another contact factor considered for the model is electric contact conductance coefficient, related to the relationship between the current density and the voltage at the contact points. The first step was to find the appropriate value of the contact stiffness which satisfies both the convergence and the accuracy requirement for the solution. Then, by adjusting the value of the electric conductance coefficient, which exert little effect on the solution in our case, the final sensing signals can be obtained. The optimum contact stiffness factor of each layer remained the same as

well as the electric conductance coefficients. Besides, the heat generation due to electric current was also defined, but it does not affect the convergence of the solution. In the solving scheme, large-deflection effects and large strain effects were included in particular for the highly nonlinear procedure.

4.2. Signal Processing and Analysis

Advanced signal processing techniques were used to extract the distinctive nonlinear features, including time-frequency analysis and wavenumber-frequency analysis. The frequency-wavenumber analysis helps decipher wave modes and frequency components in the scattered wave field. And the WDICs were adopted to depict different scattering patterns, from which the sensitive wave-path directions can be inferred for effective active sensing array design.

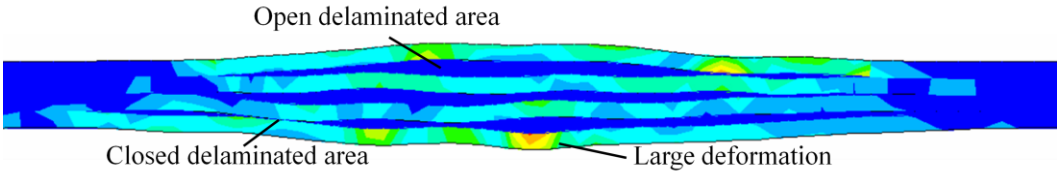

Figure 4: The wave propagation snapshot showing nonlinear interactions between guided waves and the impact damage.

Figure 4 illustrates the nonlinear wave interaction with the impact damage. Once guided waves interact with damage, mode conversion may happen and trapped modes may build up in the impact damage site. The trapped energy forms local resonances in the delaminated areas, and trapped modes may scatter and reflect within the impact damage areas. Obvious open-close contact-impact phenomenon can be observed at the delamination interfaces. This would give rise to the CAN in the sensing signals. Besides, large deformations appear in the top and bottom layers of laminates.

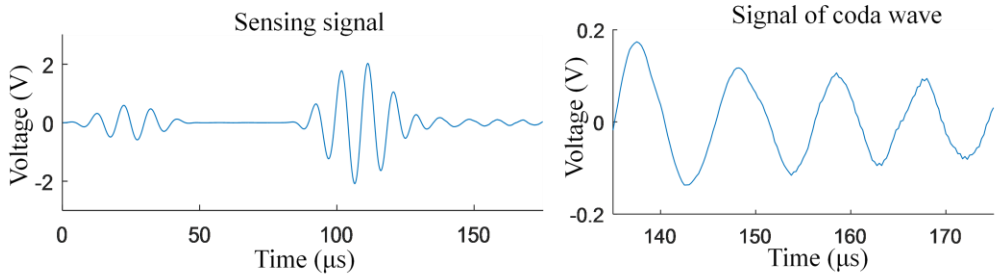

Figure 5: Sensing signals of the impact damage model.

Figure 5 shows the sensing signal of impact damage model. Two main wave packages can be observed, which are the electro-mechanical coupling signal and single S0 mode wave. After the S0 mode, coda wave also carries very rich damage information. The trapped energy would vanish with time as it slowly dissipates into the plate. The zoom-in view of the coda wave is plotted on the right side of Figure 5. The zigzags can be found

at the end of the coda wave signal due to impact damage local resonances and the contact acoustic nonlinearity among the contact surfaces.

The short time Fourier Transform (STFT) was performed on the sensing signals. The nonlinear signal components are well shown in Figure 6. Superharmonics are apparent in the frequency domain, spreading from 200 kHz to 300 kHz. After the main package, obvious local resonance can be observed in the coda wave.

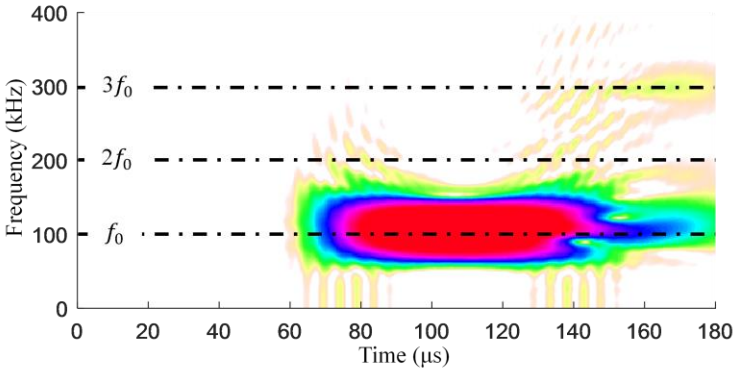

Figure 6: Time-frequency representation of a typical sensing signal.

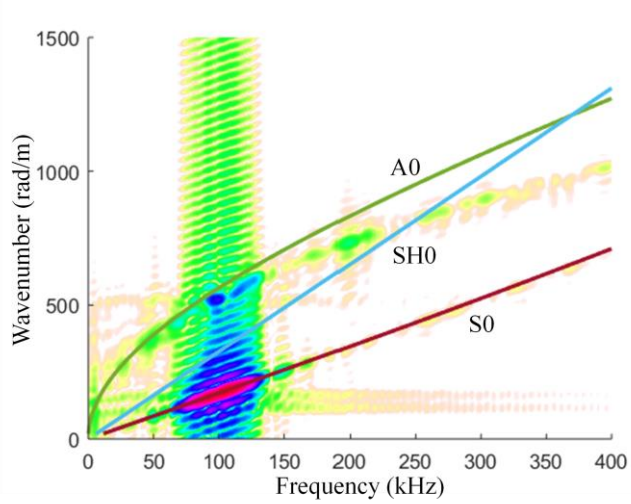

Figure 7: Frequency-wavenumber analysis of guided waves after their interaction with the impact damage.

To further excavate the nonlinear signal features, frequency wavenumber analysis was performed. Figure 7 shows the result of frequency wavenumber domain guided wave signals after interaction with the impact damage. The main energy of S0 mode at around 100 kHz can be obviously observed, concentrating on the S0 dispersion curve. While after the interacting, higher harmonic components appeared, and A0 mode guided waves were introduced due to mode conversion and can be observed across a wide frequency

span. The wavenumber analysis results overlap well with the theoretical S0 dispersion curve, with slight deviation with A0 dispersion curve. As the mesh size could not satisfy the A0 wavelength accuracy requirement at very high frequency, the deviation becomes larger for higher frequency ranges. Nevertheless, the high frequency nonlinear components are quite obvious for both S0 and A0 mode, proofing the nonlinear ultrasonic phenomenon. The analysis also demonstrates the sensitivity of the nonlinear technique for monitoring of impact damage.

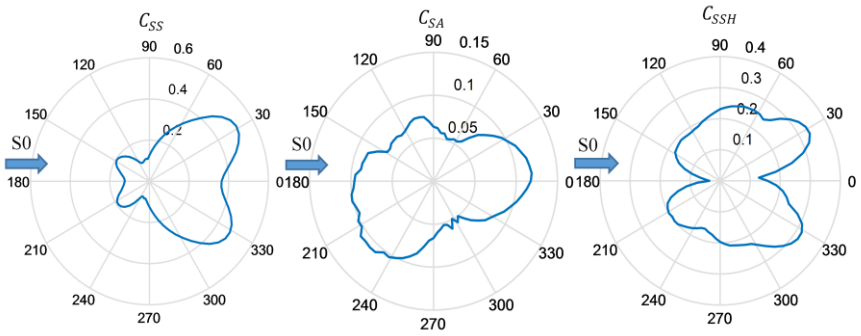

Figure 8: WDICs of S0 wave interaction with the impact damage.

In this study, the WDICs are adopted to depict the scattering patterns of guided waves, from which the sensitive wave-path directions can be inferred for active sensing array design. Figure 8 shows the WDICs of S0 wave interaction with the impact damage. C_{SS} represents the amplitude coefficients of the scattered S0 mode induced by the incident S0 mode; C_{SA} represents the amplitude coefficients of the scattered A0 mode converted from the incident S0 mode; C_{SSH} represents the amplitude coefficients of the scattered SH0 mode converted from the incident S0 mode. It can be observed that the interaction between the incident S0 wave and the impact damage not only involves scattered S0 wave, but also involves mode converted A0 and SH0 waves. Also, the amplitude coefficients are heavily direction-dependent. In general, the wave path direction is sensitive to the appearance of the impact damage for both S0 and A0 modes.

5. Virtual Time Reversal Tomography for Impact Damage Detection

Based on the impact damage model, an active sensing array was designed to capture the structural response containing the damage information. In addition, virtual time-reversal method was utilized to locate and image the impact damage.

5.1. Finite Element Model and Sensing Array Design

Figure 9 shows the finite element model constructed for the impact damage detection simulation in a 516-mm long, 516-mm wide, and 2-mm thick piezoelectric composite plate. SOLID5 coupled field element was employed to discretize the spatial domain. Extended region of ALID was implemented surrounding the plate to eliminate the boundary reflections as well as to minimize the model size. The piezoelectric composite

material was used as both the actuation and sensing components. Consequently, only surface bonded electrodes are needed at the designated actuation and sensing locations. In this study, a total number of ten actuation/sensing electrodes were used in the sensing array design. The electrodes took the circle shape with a diameter of 10 mm. And they were placed 75 mm apart from each other in two rows. Once an actuation electrode was activated, then all the five sensing electrodes in the other row were used to record the structural response. The rationale for such an array design aimed at identifying the scattered waves from the damage. The impact damage was the same as described in the impact damage model of Part 4, located at (208, 338) mm. Guided wave generated by the actuation electrode would propagate along the plate structure, then scattered from the damage site, and would finally arrive at the sensing electrodes.

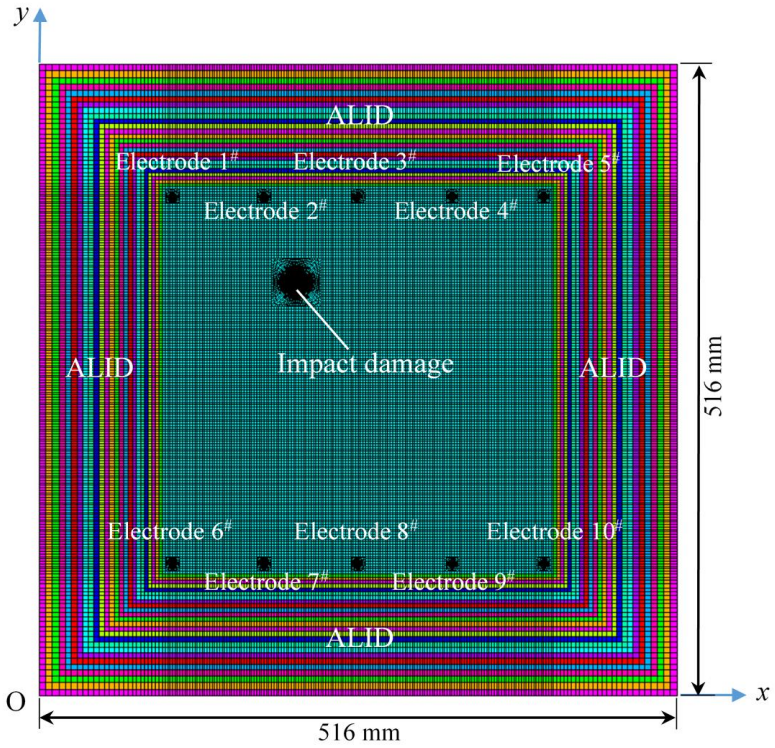

Figure 9: Finite element model with ten actuation/sensing electrodes.

Figure 10 shows the snapshot of the stress wave field excited by the actuation electrode 2#. S0 and SH0 wave modes are excited, and the wave speed of S0 mode is much higher than that of SH0 mode. The existence of SH0 mode is due to the coupling between tension, shear and bending from the material properties. Effective wave absorption at the ALID boundary can be noticed. In addition, the scattered waves from the impact damage can be clearly identified. The wave energy along the path through the impact damage is weaker than that in other directions. Because the wave energy past the impact damage would be trapped in the impact damage. The delamination became a new wave source, gradually emitting waves into the structure from the trapped local resonance.

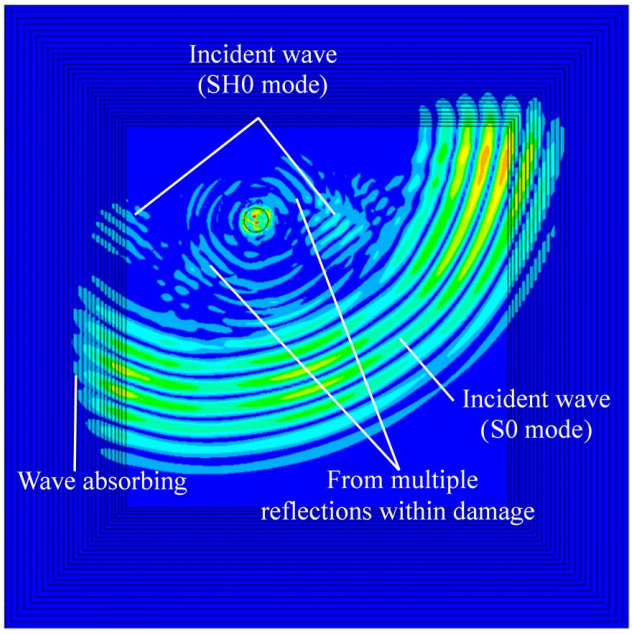

Figure 10: The wave propagation snapshot in the piezoelectric composite plate.

5.2. Virtual Time Reversal Tomography Algorithm for Damage Imaging

In VTR algorithm, it is only required to conduct the actuation-receiving procedure once in a typical pitch catch configuration. The physical time reversal procedure is replaced by a virtual computation by taking the complex conjugate of the spectrum of the sensing signal. Liu et al. [Liu (2015)] derived the final equation for VTR algorithm, given by

$$f_{B2}(\omega) = f_{B1}^{*}(\omega)\frac{f_{B1}(\omega)}{f_{A1}(\omega)} \tag{1}$$

where $f_{A1}(\omega)$ is the actuation signal in the frequency domain; $f_{B1}(\omega)$ is the sensing signal in the frequency domain; $f_{B2}(\omega)$ is the reconstructed final signal in the frequency domain; ω is the angular frequency; the superscript $*$ denotes a complex conjugate operation. The reconstructed final signal can be attained via the Inverse Fast Fourier Transform (IFFT) operation on $f_{B2}(\omega)$.

Damage identification and quantification can be accomplished by comparing the reconstructed signal against the actuation signal. When the structural damage exists in the wave path, guided waves propagating along this path may be mode-converted, reflected or scattered by the damage and linear reciprocity of the wave structure breaks down. Thus, the difference between the reconstructed signal and the actuation signal can indicate the presence of the damage without the requirement of a baseline. The damage index (DI) is defined as:

$$\mathrm{DI} = 1 - \frac{\left| \int_{t_0}^{t_1} I(t)V(t)dt \right|}{\sqrt{\int_{t_0}^{t_1} I^2(t)dt \int_{t_0}^{t_1} V^2(t)dt}} \tag{2}$$

where $I(t)$ is the excitation signal; $V(t)$ designates the reconstructed signal following the VTR algorithm; t_0 and t_1 define the time interval over which the signals are compared. In this paper, t_0 and t_1 are respectively the starting and ending points of the time reversal interception window.

The probability of damage occurrence at position (x, y) in each direction produced from the path of each actuation and sensing pair are added directly. The final VTR probabilistic imaging algorithm can be express as

$$P(x,y) = \sum_{m=1}^{M} \sum_{n=1}^{N_m} DI_{mn} E(R_{mn}(x,y)) \tag{3}$$

where $P(x,y)$ denotes the probability of damage occurrence at the position (x, y); M is the number of actuation electrodes, and in this case it should be ten; N_m is the number of sensing electrodes for each actuation electrode m, and in this cause it should be five; subscript mn indicates the sensing signal from n_{th} sensing electrode generate by actuation electrode m.; DI represents the results expressed by Eq. 2; $R_{mn}(x,y)$ is defined as the distance between the position (x, y) and the path of each actuation and sensing electrodes pair; $E(R_{mn}(x,y))$ is the Gaussian decreasing function to estimate the energy distribution of the interrogating wave ray and can be formulated as:

$$E(R_{mn}(x,y)) = \begin{cases} \frac{1}{\sigma\sqrt{2\pi}} e^{-(\frac{R_{mn}(x,y)}{D})/2\sigma^2} & R_{mn}(x,y) \le D, \\ 0 & R_{mn}(x,y) > D, \end{cases} \tag{4}$$

where D determines the width of interrogating wave ray and σ defines the decreasing ratio of Gaussian function. Herein, the parameters D and σ are chosen as 50 mm and 0.6.

5.3. Signal Post-Processing and Tomography Imaging Result

In order to eliminate the tuning effect on the final imaging result, before performing the IFFT operations, the frequency domain of reconstructed signals are processed to diminish the tuning influence indicated in Section 3. The tuning procedure would inevitably change the frequency components of the excitation signal. Thus, a compensation procedure was carried out to eliminate the tuning effect for the purpose of distinguishing the influence from the impact damage.

Figure 11 shows the post-processing results of two particular paths, one deviated from the damage zone, the other passing the damage site. It can be obviously noticed that when the

generated wavefield does not interact with the impact damage, the reconstructed signal agrees well with the excited signal. However, when the damage resides on the sensing path, the main frequency components experience an obvious shift because of the wave trapping effect and CAN involving the nonlinear phenomenon. Once using VTR algorithm, the high-frequency components will dominate in the spectrum of the reconstructed signal. Consequently, the reconstructed signal exhibits high frequency oscillations. This further demonstrates the superb sensitivity of nonlinear ultrasonics for impact damage detection. Based on the reconstructed signals, the final image of the piezoelectric composite plate can be attained.

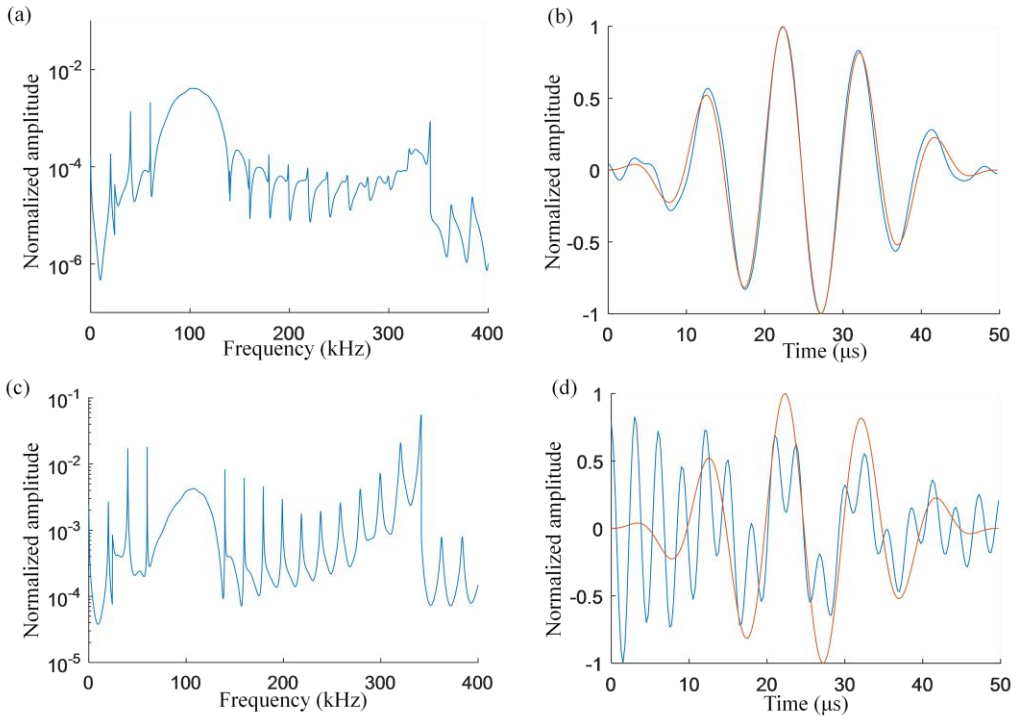

Figure 11: Reconstructed signals: (a) spectrum of reconstructed signal of path $1^{\#}$-$6^{\#}$; (b) reconstructed signal of path $1^{\#}$-$6^{\#}$ compared with the excitation; (c) spectrum of reconstructed signal of path $2^{\#}$-$9^{\#}$; (d) reconstructed signal of path $2^{\#}$-$9^{\#}$ compared with the excitation (blue line: reconstructed signal; orange line: excitation).

Figure 12 presents the VTR probabilistic tomography imaging result for impact damage detection. Remarkable accuracy is achieved for damage localization and imaging, as the maximum pixel position in the image is at (207, 340) mm, only 0.2% and 0.4% deviation compared to the actual damage position in the finite element model indicated by the black circle in Figure 12.

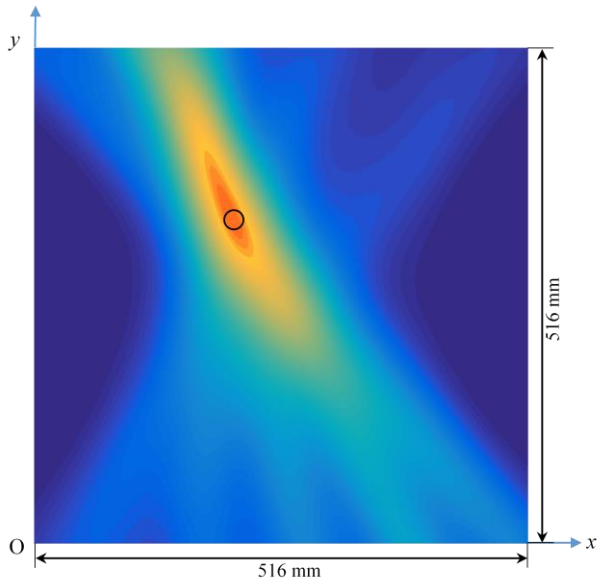

Figure 12: VTR probabilistic tomography imaging result for impact damage detection.

6. Summary, Concluding Remarks, and Suggestions for Future Work

This paper presented the virtual time reversal tomography for impact damage detection in self-sensing piezoelectric composite plates. Dispersion relations of guided waves were obtained with finite element modal analysis, and the group velocity directivity curves of three fundamental modes were determined. Through the electrodes tuning study, the guided wave generation and reception characteristics were obtained, which facilitates the selection of the actuation frequency in the transient dynamic simulation and experiment.

Impact damage were introduced and modelled as a group of cone shape delaminations and stiffness losses within the layers through the thickness direction. In addition, contact dynamics were considered to capture the possible nonlinear interactions between guided waves and the impact damage. Using time frequency and frequency wavenumber analysis, mode conversion and local resonances at the damage were illustrated. Furthermore, the wave damage interaction coefficients depicted scattering patterns of guided waves, from which the sensitive wave-path directions can be inferred for active sensing array design. Finally, the predictive simulation signals from the 3D finite element models were fed into the virtual time-reversal probabilistic imaging algorithm. It was found that the VTR tomography approach can effectively detect and image the impact damage. The piezoelectric composite material shows its great potential for establishing structural self-awareness and may be applied in future engineering structures.

It should be noticed that the numerical investigation was based on the assumption of special stiffness and piezoelectric property. Thus, it is necessary to attain them from future experiments. Future work should focus on the experimental tests and SHM system design using such piezoelectric composite plates.

Acknowledgement: The support from the National Natural Science Foundation of China (contract number 51605284) is thankfully acknowledged.

References

Aberg, M.; Gudmundson, P. (1997): The usage of standard finite element codes for computation of dispersion relations in materials with periodic microstructure. *Journal of the Acoustical Society of America*, vol. 102, no. 102, pp. 2007-2013.

Aymerich, F.; and Staszewski, W. J. (2010): Impact damage detection in composite laminates using nonlinear acoustics. *Composites Part A: Applied Science & Manufacturing*, vol. 41, no. 9, pp. 1084-1092.

Cai, J.; Shi, L.; Yuan, S.; Shao, Z. (2011): High spatial resolution imaging for structural health monitoring based on virtual time reversal. *Smart Materials & Structures*, vol. 20, no. 5, pp. 55018-55028.

Giurgiutiu, V. (2005): Tuned Lamb wave excitation and detection with piezoelectric wafer active sensors for structural health monitoring. *Journal of Intelligent Material and Structures*, vol. 16, pp. 291-305.

Haghiashtiani. G.; Greminger, M. A. (2015): Fabrication, polarization, and characterization of PVDF matrix composites for integrated structural load sensing. *Smart Materials & Structures*, vol. 24, no. 4, pp. 45038-45048.

Liu, Z.; Yu, H.; Fan, J.; Hu, Y.; He, C.; Wu, B. (2015): Baseline-free delamination inspection in composite plates by synthesizing non-contact air-coupled Lamb wave scan method and virtual time reversal algorithm. *Smart Materials & Structures*, vol. 24, no. 4, pp. 45014-45028.

Minakuchi, S.; Takeda, N. (2013): Recent advancement in optical fiber sensing for aerospace composite structures. *Photonic Sensors*, vol. 3, no. 4, pp. 345-354.

Patra, S.; Banerjee, S. (2017): Material state awareness for composite part I: precursor damage analysis using ultrasonic guided code wave interferometry (CWI). *Materials*, vol. 10, no. 12, pp. 1436-1451.

Wang, J.; Shen, Y. (2018): Numerical investigation of ultrasonic guided wave dynamics in piezoelectric composite plates for establish structural self-sensing. *Journal of Shanghai Jiao Tong University*, vol. 23, no. 1, pp. 175-181.

Zhu, K.; Fang, D. (2014): Calculation of dispersion curves for arbitrary waveguides using finite element method. *International Journal of Applied Mechanics*, vol. 6, no. 5, pp. 1450059-1-12.